Korean Journal of Remote Sensing, Vol.23, No.5, 2007, pp.421~430

Estimation of Ocean Current Velocity near Incheon using Radarsat-1 SAR and HF-radar Data

Moon-Kyung Kang and Hoonyol Lee †

Department of Geophysics, Kangwon National University

Abstract : This paper presents the results of the ocean surface current velocity estimation using 6 Radarsat-1 SAR images acquired in west coastal area near Incheon. We extracted the surface velocity from SAR images based on the Doppler shift approach in which the azimuth frequency shift is related to the motion of surface target in the radar direction. The Doppler shift was measured by the difference between the Doppler centroid estimated in the range-compressed, azimuth-frequency domain and the nominal Doppler centroid used during the SAR focusing process. The extracted SAR current velocities were statistically compared with the current velocities from the high frequency (HF) radar in terms of averages, standard deviations, and root mean square errors. The problem of the unreliable nominal Doppler centroid for the estimation of the SAR current velocity was corrected by subtracting the difference of averages between SAR and HF-radar current velocities from the SAR current velocity. The corrected SAR current velocity inherits the average of HF-radar data while maintaining high-resolution nature of the original SAR data.

Key Words : SAR, ocean current, velocity, HF-radar, Doppler shift.

1. Introduction

For the last several decades, a variety of spaceborne optical and radar observation have revealed surface characteristics related to the dynamic phenomena over the ocean. A good understanding of ocean surface condition is essential for any activity connected with the sea, e.g., fisheries, ship routing, coastal surveillance, offshore drilling and exploration, aquaculture, environmental monitoring, and coastal engineering (Mouchot and Garello, 1998). Many researchers have investigated the oceanographic applications of SAR system that allows the detection of various oceanic features such as waves, currents, internal waves, winds, oil spills and ship wakes with high resolution ocean images regardless weather conditions, day and night (Elachi, 1988).

Unlike the target on the land, the radar scattering mechanism over the ocean must be taken into account the sea surface motion as well as its roughness and dielectric constant. Moving targets over the ocean cause the Doppler shift of the backscattered radar signal, proportional to the target's line-of-sight velocity. Ocean surface current velocity

Received 4 October 2007; Accepted 17 October 2007.

† Corresponding Author: Hoonyol Lee (hoonyol@kangwon.ac.kr)

can be evaluated by estimating the Doppler frequency of the SAR data. The Doppler shift can be measured by estimating the difference of the Doppler centroid obtained from the SAR data and the nominal Doppler centroid calculated by using the trajectory parameters of satellite orbit.

The purpose of this study is 1) the estimation of ocean current velocity from SAR images using the Doppler shift method and 2) the evaluation and correction of the results by comparing them with HF-radar data.

2. Methodology

1) Study Area and Data

The study area is located near Incheon in the west coast of Korean peninsula (Fig. 1) where the tidal current speed is much higher than that of the eastern or southern coast of Korea.

Total 6 Radarsat-1 SAR images were used in this study that were acquired in May 6 and 30, July 17, August 10, September 27, and October 21, 2003, respectively. The Radarsat-1 SAR operated at C-band (5.3 GHz) in HH polarization, and the images used in this study were all in ascending orbit, standard mode 5 with approximately 39° of incidence angle, as listed in Table 1.

Table 1. Characteristics of the Radarsat-1 SAR images.

Date (mm/dd/yyyy)	Local Time (hh:mm:ss)	Scene Center (deg)	Incidence Angle (deg)
05/06/2003	18:33:25	37.0139093 N, 126.3653691 E	39.172
05/30/2003	18:33:22	37.0389203 N, 126.2102356 E	39.173
07/17/2003	18:33:17	37.0204028 N, 126.3696765 E	39.164
08/10/2003	18:33:14	37.0206934 N, 126.3721770 E	39.163
09/27/2003	18:33:13	37.0155422 N, 126.3608840 E	39.153
10/21/2003	18:32:58	36.9946995 N, 126.3659331 E	39.157

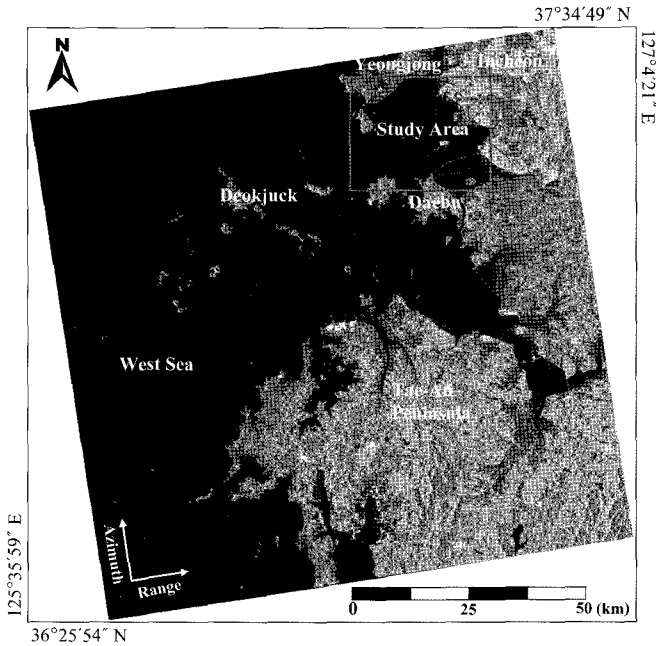

Fig. 1. The location of study area depicted in a Radarsat-1 SAR image.

The HF-radar data used in this work were measured by National Oceanographic Research Institute (NORI) of Korea at the same time of SAR data acquisition and also in the West Sea between 37°17′ 34″ to 37° 28′ 7″ N and 126°25′ 7″ to 126°36′ 52″ E. It gives the current velocity data in east and north direction.

2) SAR Current Velocity

For the estimation of the surface velocity from SAR images, we used the SAR Ocean Processor (SOP) developed by Kangwon National University (Kang *et al.*, 2007) shown in Fig. 2. The overall procedure for the estimation of the surface current velocity from Radarsat-1 SAR images and HF-radar data is outlined in Fig. 3.

The aims of the SOP are the extraction of ocean wind, wave, and current parameters from SAR images. The SOP works at cygwin (www.cygwin.com) environment and the output files of the SOP are produced separately for the wind, wave, and current information. Table 2 lists the inputs and outputs of the

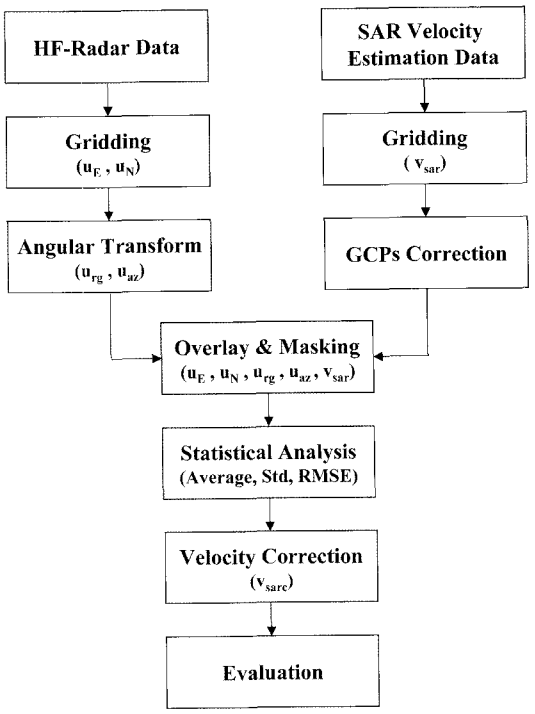

Fig. 3. The overall procedure for estimating the surface current velocity from SAR and HF-radar data.

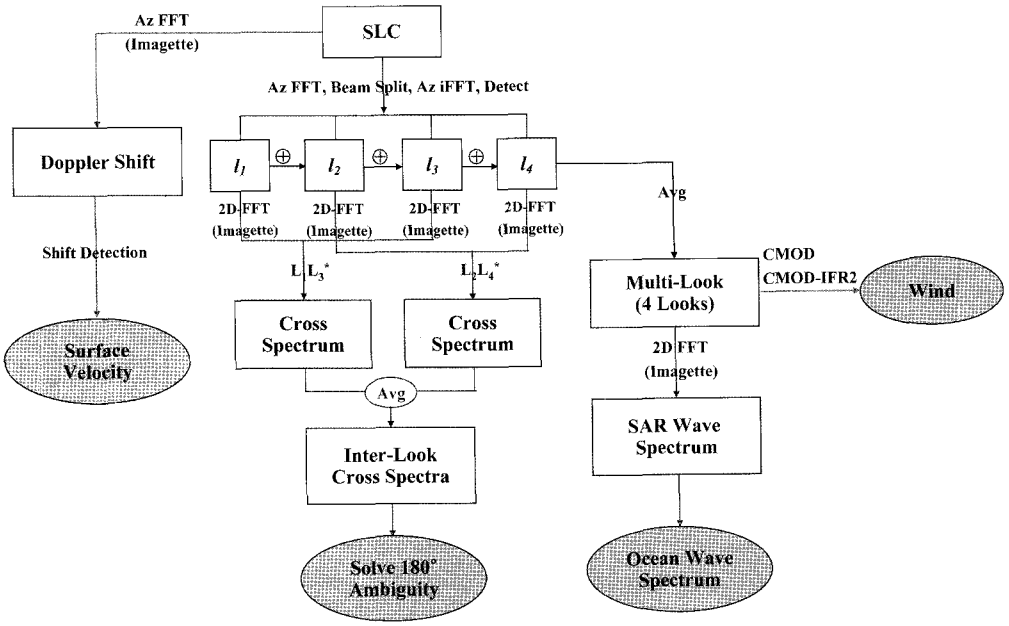

Fig. 2. The flow chart of the SAR Ocean Processor (SOP) (Kang *et al.*, 2007).

Table 2. The inputs and outputs of the SOP (Kang *et al.*, 2007).

Input		• Radarsat-1 SLC (CEOS Format)
Output	SLC	• Single-Look Complex (Header Off)
	ML	• Multi-Look Image (by Average)
	Wind	• Backscattering Coefficient (dB) • CMOD4 Wind Speed (m/s) • CMOD-IFR2 Wind Speed (m/s)
	Wave	• SAR Wave Spectrum • Inter-Look Cross Spectrum • Multi-Look Image (Inter-Look Processing)
	Current	• Doppler Image • Doppler Shift Estimation (Vector File) • Velocity Estimation (Text File) • Velocity Estimation Vectors (Vector File)

SOP. The SOP implemented the existing algorithms such as the CMOD4 (Stoffelen and Anderson, 1997a, 1997b), CMOD-IFR2 (IFREMER-CERSAR, 1999) models, and a polarization ratio conversion (Horstmann *et al.*, 2000) for the retrieval of wind speed, the wave-SAR transforms and inter-look cross-spectra (Engen and Johnsen, 1995) for the extraction of wavelength and propagation direction of wave, and the Doppler shift approach (Chapron *et al.*, 2005) for the estimation of the surface current velocity. Only the surface current velocity is extracted by the SOP and evaluated in this paper as it is a dominant oceanic phenomenon in this study area driven by the strong tidal current.

The surface velocity, V_D for a simple target of fixed shape moving toward the radar line-of-sight can be calculated as (Chapron *et al.* 2005)

$$V_D = f_D / k_e \sin\theta_I \quad (1)$$

where f_D is the Doppler shift of the surface target, k_e is the wavenumber of the incident electromagnetic wave, and θ_I is the incidence angle of the radar beam. f_D can be calculated by multiplying Δf by $\Delta pixel$, where Δf is the frequency sampling interval and $\Delta pixel$ is the pixel distance between the nominal and the estimated Doppler centroid in the azimuth frequency domain. V_D and f_D are defined positive if the target moves toward the radar.

Table 3. The optimization for input parameters of the SOP.

Parameters (SOP)	Considered Value	Optimized Value
nptyc	64, 128, 256	128
dc_xstep (=*dc_ystep*)	32, 64, 128, 256	32
dc_avx × *dc_avy*	(5 to 21) × (17 to 81)	21 × 81
vel_scale	100 ~ 1000	300 ~ 900

Table 3 shows the major input parameters of the SOP for extracting surface velocity are *nptyc* for 1D azimuth FFT size, *dc_xstep* and *dc_ystep* for current estimation steps, *dc_avx* and *dc_avy* for averaging factor during Doppler center estimation (all in pixel dimension), and *vel_scale* for velocity vector scale during display (pixel/sec). The *nptyc*, *dc_avx*, and *dc_avy* have direct influenced on the quality of the surface velocity measurement, which have to be chosen carefully by a certain optimization procedure, while the *dc_xstep*, *dc_ystep*, and *vel_scale* parameters give variety in vector display.

The estimated SAR current velocity vectors were converted into a grid map and then geocoded by using the ground control points (GCPs). The geocoded raster images of SAR current velocity is overlaid with the current velocity raster images of HF-radar prepared by the following procedure.

3) HF-Radar Current Velocity

The current velocity of HF-radar was observed in two directions: eastward and northern direction. The measured HF-radar data were in text format files that should be changed to grid map for subsequent image processing. As the SAR current velocity extracted from the SOP is in range direction only, the HF-radar current velocity should be rotated to range and azimuth directions for comparison. Fig. 4 shows the relation between the original coordinates (eastward and northern) of HF-radar and the rotated coordinates (range and azimuth). The rotation of coordinates can

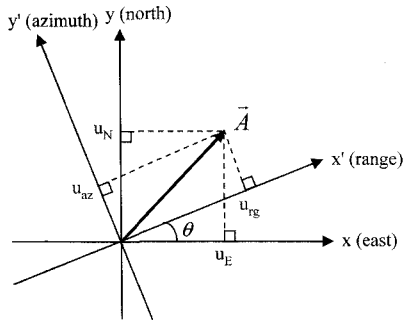

Fig. 4. Geometry illustrating angular transformation from the north-east to range-azimuth coordinates.

be done by the following formula:

$$\begin{pmatrix} u_{rg} \\ u_{az} \end{pmatrix} = \begin{pmatrix} \cos\theta & \sin\theta \\ -\sin\theta & \cos\theta \end{pmatrix} \begin{pmatrix} u_E \\ u_N \end{pmatrix} \quad (2)$$

where,

u_E : eastward current velocity (m/s)

u_N : northern current velocity (m/s)

u_{rg} : current velocity transformed toward range direction (m/s)

u_{az} : current velocity transformed toward azimuth direction (m/s)

θ : angle between eastward direction and range direction

4) Statistical Analysis and Correction

The geocoded map of the SAR and HF-radar current velocities were overlaid and masked out so that the area includes the ocean surface only and keeps a good distance from the lands nearby. The velocities from HF-radar in range direction (u_{rg}) and SAR image data (v_{sar}) were compared and analyzed by the statistical method such as averages, standard deviations, and root mean square (RMS) errors. Assuming the HF-radar data as a reference, the SAR velocity was corrected (v_{sarc}) accordingly. More details on the correction method will be described and justified in the later section.

3. Results

Firstly, the parameter optimization for the SOP processing has been performed based on the statistical test on the results from various parameter sets. The Radarsat-1 SAR images listed in Table 4 were then processed using the optimized SOP parameters. The results then compared with the HF-radar data and then a correction procedure has been implemented to complement the possible errors in the nominal Doppler centroid during SAR focusing.

1) Optimization of SOP Parameters

Fig. 5 shows an example of the SAR current velocity image obtained in July 17, 2003 with varying averaging window size of *dc_avx* from 5 to 21 and *dc_avy* from 17 to 81. As shown in Fig. 5 (b) to (f), the graphical distribution of SAR current velocity becomes similar to the HF-radar current velocity (u_{rg}) shown in Fig. 7(c). This indicates that the large size of the averaging window during the Doppler centroid estimation is necessary to overcome the noise effect of the azimuth-frequency data.

According to SAR principle, the radar beam shape that has the maximum amplitude in the center and degrades along the azimuth direction in a bell-shaped style is visible in an image in range-compressed time and azimuth-frequency domain. By finding a frequency value that gives the maximum amplitude, one can estimate the Doppler centroid and thus the Doppler shift from the nominal Doppler centroid calculated from the satellite's state vectors.

Fig. 6 shows the statistical graphs of the averages and standard deviations of the SAR current velocities with increasing size of averaging window (*dc_avx* and *dc_avy*). The standard deviation values were generally high when a relatively small averaging window is used for Doppler estimation procedure. This is because of the noisy nature of the azimuth-

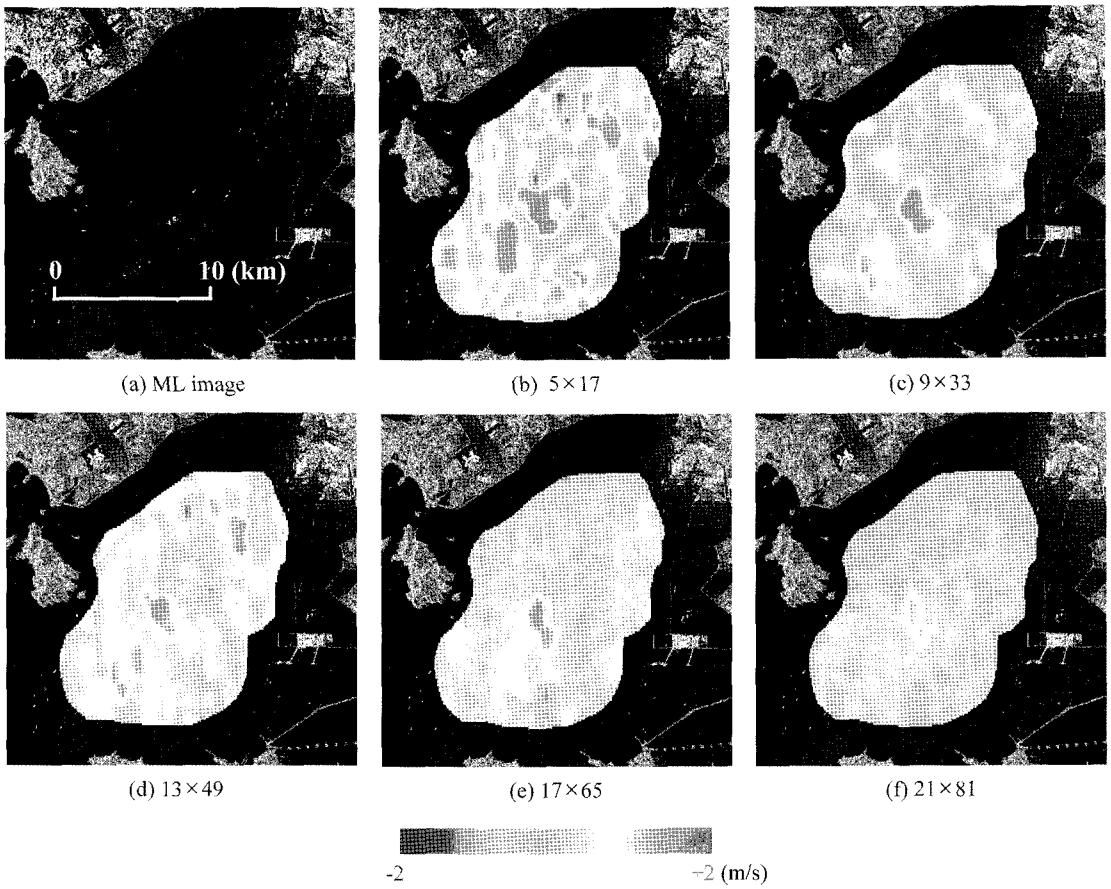

Fig. 5. Examples of the SAR current velocity (colored region, m/s) with varying *dc_avx* × *dc_avy* (July 17, 2003).

frequency data that makes the estimation process to easily fall into a local minimum. This local-minimum problem during the estimation process can be overcome by enlarging the size of the average window thus to smooth the data field. By doing so, the Doppler centroid can be effectively detected by choosing the frequency value that gives the maximum amplitude out of the typically bell-shaped beam model in the azimuth-frequency domain at the expense of resolution. Therefore, the averaging window is a trade off between the estimation accuracy of Doppler centroid and the resolution.

As the tidal current velocity is relatively homogeneous in the study area, it is also expected that the standard deviation of the current velocity should have a small value, and less sensitive to the averaging window size. Therefore, we determined the optimal size of the averaging window by the value that the standard deviation becomes stabilized in Fig. 6. From the analysis of the statistical distribution, we selected the optimal averaging window with *dc_avx* and *dc_avy* of 21 by 81, respectively, and used it for the rest of the Radarsat-1 SAR images. The spatial resolution of the current estimation corresponds to approximately 300 m × 300 m in this case.

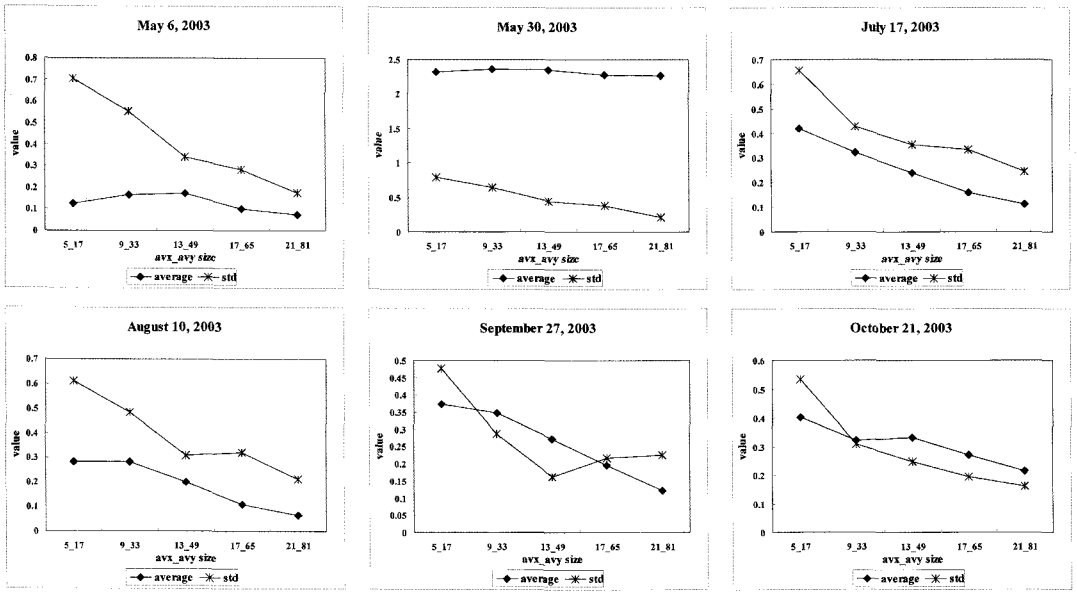

Fig. 6. Change of averages and standard deviations of the SAR current velocity as a function of varying averaging window size defined by *dc_avx* × *dc_avy*.

2) Comparison between the SAR and HF-radar Current Velocities

Table 4 lists the statistical values of the SAR and HF-radar current velocities such as averages, standard deviations and RMS errors. The sign of averages is positive (+) for flood tide and negative (-) for ebb tide. Fig. 7 exhibits the image sets of the SAR current velocity (first column) and the HF-radar current velocity (second column). The flood tide is in yellow color and the ebb tide appears cyan.

The average values of SAR current velocities show a considerable difference when compared with the corresponding HF-radar current velocities. The gap was very high especially on May 30, 2003, where the SAR current velocity indicated unusually high flood tide while the HF-radar current velocity indicates ebb tide. It is evident that there exists a big difference in average values between the SAR and HF-radar data that contributes a lot to the RMS errors while the standard deviation is relatively small. It is postulated that a constant difference in averages of the SAR and HF-radar current velocities can be produced when there is uncertainty in the nominal Doppler centroid estimation during the SAR focusing. The nominal

Table 4. Statistical analysis of the current velocities from SAR and HF-radar.

Velocity / Date	SAR Velocity (v_{sar})		HF-Radar (u_{rg})		Difference ($v_{sar} - u_{rg}$)			Corrected SAR Velocity (v_{sarc})	
	Avg.	Std	Avg.	Std	Avg.	Std	RMSE	Avg.	Std
05/06/2003	0.08	0.18	0.18	0.11	-0.10	0.17	0.20	0.18	0.18
05/30/2003	2.27	0.21	-0.36	0.10	2.63	0.23	2.64	-0.36	0.21
07/17/2003	0.11	0.25	0.33	0.13	-0.22	0.27	0.35	0.33	0.25
08/10/2003	0.07	0.21	-0.48	0.19	0.55	0.33	0.64	-0.48	0.21
09/27/2003	0.12	0.23	-0.13	0.14	0.25	0.23	0.34	-0.13	0.23
10/21/2003	0.22	0.16	-0.29	0.14	0.51	0.21	0.55	-0.29	0.16

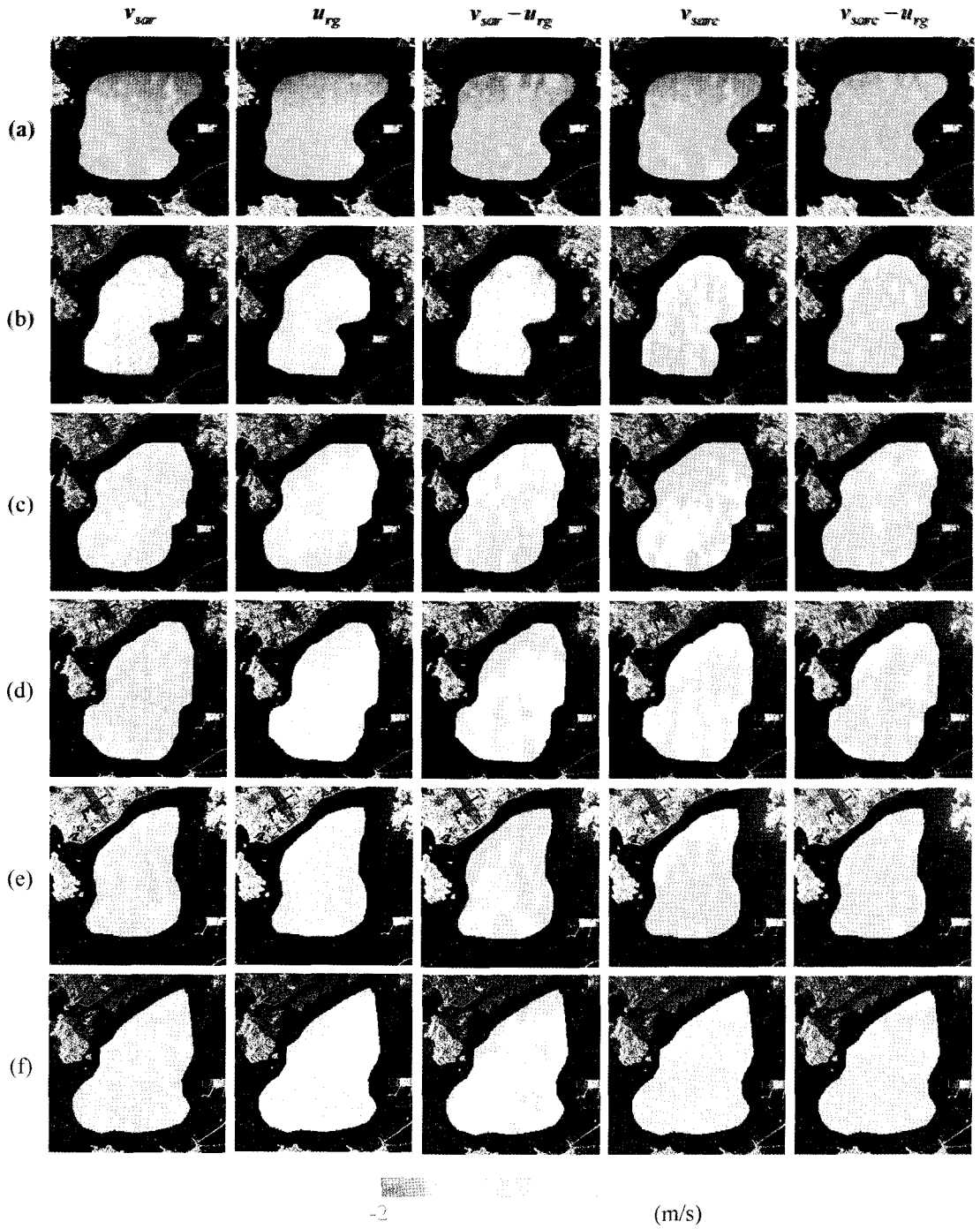

Fig. 7. Ocean current velocity maps in range direction (m/s). The acquisition dates of the Radarsat-1 SAR images are (a) May 6, (b) May 30, (c) July 17, (d) August 10, (e) September 27, and (f) October 21, 2003. The 1st column is the SAR current velocity (v_{sar}) and the 2nd is the HF-radar current velocity (u_{rg}). The 3rd column is v_{sar} - u_{rg}. The 4th is the corrected SAR current velocity (v_{sarc}) and the 5th is v_{sarc} - u_{rg}.

Doppler centroid is calculated from the satellite's state vectors such as the position and velocity vectors with time, which is generally acceptable for general SAR processing (Curlander and McDonough, 1991; Lee, 2005) but not for the purpose of the velocity estimation causing significant errors. Therefore, we tried to correct the current velocity anomaly of constant type caused by the uncertainty of the nominal Doppler centroid, by using the difference of averages between the SAR and HF-radar current velocities.

3) Correction of the SAR Current Velocity

To compensate for the possible errors caused by the nominal Doppler centroid, the difference of averages between the current velocities from SAR and HF-radar was subtracted from the SAR current velocity as:

$$v_{sarc} = v_{sar} - (\bar{v}_{sar} - \bar{u}_{rg}) \quad (3)$$

The images of the corrected SAR current velocity (v_{sarc}) are shown in the 4th column of Fig. 7 and also the statistics in Table 4. After the correction, the SAR current velocity images (4th columns) are much similar to the HF-radar current images (2nd column). There is also a significant improvement in the difference images before (3rd column) and after the correction (5th column). In case of the difference images, red color appear when the SAR velocity is higher than the current velocity of HF-radar and the blue color is for the opposite. From this result we confirmed that the nominal Doppler centroid anomaly during SAR focusing processing can be corrected by using the reference data such as the HF-radar current velocity data.

Table 4 shows that the corrected SAR current velocity (v_{sarc}) inherits the average of the HF-radar current velocity (u_{rg}) and the standard deviation of the SAR current velocity before correction (v_{sar}). This means that a constant error in the nominal Doppler centroid has been corrected by the HF-radar data while the advantage of higher resolution of the SAR current velocity has been maintained.

4. Conclusion

This study presented the results of estimating the ocean surface current in West Sea near Incheon of Korea by using Radarsat-1 SAR images and HF-radar data. The retrieval of current velocity from SAR images was processed by the SOP program based on the Doppler shift approach. The extracted SAR current velocity was compared with the HF-radar current velocity by statistical method such as averages, standard deviations, and RMS errors. We concluded that 1) the problem related to the unreliable nominal Doppler centroid estimation during the SAR focusing can be corrected by a reference data such as the HF-radar data; 2) the corrected SAR current velocity has the average of HF-radar data while maintaining the advantage of high-resolution SAR.

Acknowledgements

This work was supported by the Korea Research Foundation Grant funded by the Korean Government(MOEHRD) (KRF-2006-351-D00043). The HF-radar data were provided by the National Oceanographic Research Institute (NORI) of Korea. The authors appreciate Ji-Hye Kang and Su-Jung Jung of the RS/GIS laboratory at Kangwon National University for their considerable assistance in data processing.

References

Chapron, B., C. Fabrice, and A. Fabrice, 2005. Direct Measurments of Ocean Surface Velocity from Space: Interpretation and Validation, *J. of Geophysical Research*, 110: 1-17.

Curlander, J. and R. McDonough, 1991. Synthetic Aperture Radar: Systems and Signal Processing, *John Wiley & Sons, Inc.*, New York.

Elachi, C., 1988. Spaceborne Radar Remote Sensing: Applications and Techniques, *IEEE Press*, New York.

Engen, G. and H. Johnsen, 1995. SAR-Ocean Wave Inversion Using Image Cross Spectra, *IEEE Transaction on Antennas and Propagation*, 33(4): 1047-1056.

Horstmann, J., W. Koch, S. Lehner, and R. Tonboe, 2000. Wind Retrieval over the Ocean using Synthetic Aperture Radar with C-band HH Polarization, *IEEE Transaction on Geoscience and Remote Sensing*, 38(5): 2122-2131.

IFREMER-CERSAR, 1999. Off-Line Wind Scatterometer ERS Products: User Manual, Technical Report C2-MUT-W-010IF, *IFREMER- CERSAR.*

Kang, M. K., Y. W. Park, M. J. Lee, and H. Y. Lee, 2007. Study on the Extraction of Ocean Wind, Wave and Current using SAR, *Journal of Korean Navigation and Port Research*, 31(1): 35-42.

Lee, H., 2005. Development and Distribution of an Educational Synthetic Aperture Radar (eSAR) Processor, *Korean Journal of Remote Sensing*, 21(2): 163-171.

Mouchot, M. -C. and R. Garello, 1998. SAR for Oceanography, in Henderson, F. M. and A. J. Lewis Ed., Principles & Applications of Imaging Radar, *John Wiley & Sons, Inc.*, New York.

Stoffelen, A. and D. Anderson, 1997a. Scatterometer Data Interpretation: Estimation and Validation of the Transfer Function CMOD4, *J. of Geophysical Research*, 102(C3): 5767-5780.

Stoffelen, A. and D. Anderson, 1997b. Scatterometer Data Interpretation: Measurement Space and Inversion, *J. of Atmospheric and Oceanic Technology*, 14: 1298-1313.